Eur. Phys. J. Plus (2023) 138:828
https://doi.org/10.1140/epjp/s13360-023-04452-w

THE EUROPEAN PHYSICAL JOURNAL PLUS

Regular Article

Distribution maps and hazard of radioelements from granitic rocks in an Egypt region

Sherif A. Taalab[1], Waheed H. Mohamed[1], Ahmed M. Abdel-Rahman[1], Mohammed S. Alqahtani[2,6,7], Giuseppe La Verde[3], Mariagabriella Pugliese[3], Mohamed Y. Hanfi[4,5,a], Fabrizio Ambrosino[3]

[1] Department of Geology, Faculty of Science, Al-Azhar University, Cairo, Egypt
[2] Radiological Science Department, College of Applied Medical Science, King Khalid University, Abha, Saudi Arabia
[3] Department of Physics "Ettore Pancini", University of Naples, Naples, Italy
[4] Nuclear Materials Authority, P.O. Box 530, El Maadi, Cairo, Egypt
[5] Institute of Physics and Technology, Ural Federal University, Yekaterinburg, Russia
[6] BioImaging Unit, Space Research Centre, Michael Atiyah Building, University of Leicester, LE1 7RH Leicester, UK
[7] Research Center for Advanced Materials Sciences (RCAMS), King Khalid University, P.O.Box 9004, 61413 Abha, Saudi Arabia

Received: 10 July 2023 / Accepted: 8 September 2023

Abstract The distribution maps of natural radioelement (^{40}K, ^{232}Th and ^{238}U) over the Wadi El Bohlog–Wadi Kam Amiri region of Egypt desert were shown. Granitic rocks, characteristic building materials of the study region, were analyzed: (1) the radionuclides contents were determined by using NaI detector; (2) minerals were investigated by an environmental scan electron microscope (ESEM). The average values of ^{238}U, ^{232}Th, ^{40}K are higher than the worldwide average. This is due to the main mineral composition of the granitic rock samples, like thorite, uranothorite, kasolite, zircon and xenotime. Radiological hazards indexes were computed to evaluate the radioactive risk of these rocks to the public, showing high values exceeding the worldwide limits.

1 Introduction

The most prominent sources of natural radioactivity are terrestrial and cosmic radiation. The two main types of exposure comes from internal exposure resulting from inhalation of radon gas and its decay products, and external exposure from gamma rays emitted by terrestrial radionuclides including ^{238}U, ^{232}Th and ^{40}K [1–3]. The Wadi El Bohlog–Wadi Kam Amiri region (latitude 26°15' N and 33° 30' E) is part of the desert of Egypt, accessible by the road Qena-Safaga, about 150 km far from the main city of Luxor. In the work [4] were examined the uranium sources in rocks characteristics of the Wadi El Bohlog–Wadi Kam Amiri region, which has two different concentric granitic magmas, i.e., composite intrusions, arranged in concentric rings, made up of granitic rocks with different geochemical characters. This granitic body exhibits hydrothermal alterations resulting in the dissolution of magmatic quartz (episyenitization) followed by other types of alterations. The main alteration features are chloritization, muscovitization, hematitization, sericitization, kaolinization, albitization, silicification, and saussuritization [5]. It is demonstrated that the key variables regulating uranium mobilization in these changeable granitic environments were pH fluctuations, oxidation-reducing conditions, mineralogical components, along with alteration processes [5, 6]. Uranium is found in nature in two oxidation states (U^{4+} and U^{6+}), with the soluble U^{6+} form dominating the Earth's surface. Thorium is mostly found in the 4 + oxidation state in terrestrial material; it is insoluble in natural water and usually carried by minerals or adsorbed to particles [7]. Unlike uranium, thorium is not absorbed into secondary carbonates during production, resulting in a Th/U disequilibrium at first [8]. ^{40}K is a natural radionuclide that also emits gamma radiation. Distribution of uranium and thorium in minerals and rocks of igneous origin can be explained in terms of crystal chemistry of the elements [9]. The geochemical coherence of U and Th during the magmatic cycle arises out of the marked similarity in their charges and ionic radii (U^{4+}, 1.05A^{O}&Th^{4+}, 1.10A^{O}). There is a relationship between uranium and the volatile components of magmas, i.e., uranium tends to concentrate in an acidic melt rich fluorine and chlorine. This behavior may explain the late precipitation of uranium in many granites. The granitic rocks from the Wadi El Bohlog–Wadi Kam Amiri region are widespread throughout the Egypt used as building materials. For assessing the radiological dangers to human health and for the correct usage and management of these rocks, it is critical to determine the concentration of radionuclides. The investigation of natural radioactivity in rocks from different worldwide locations used in building construction is common practice [10–13]. The main objective of the present work is to determine the factors influencing radioactivity and mineralogy in granitic rocks from the Wadi El Bohlog–Wadi Kam Amiri region, together with the assessment of the radiological hazard indexes associated with these rocks.

[a] e-mails: mokhamed.khanfi@urfu.ru; m.nuc2012@gmail.com (corresponding author)

Published online: 21 September 2023

2 Materials and methods

2.1 Geologic map of the study area

The Egyptian granites are classified into older and younger granites. The older granites of the Eastern Desert (ED) constitute about 27% it's basement outcrops [14]. They occur as low relief igneous mountains. They intrude the oldest rock types such as metavolcanics, and metasediments and have commonly have foliated margins concordant to wall rock structure. The older granites (OG) are metaluminous to slightly peraluminous, and have calc-alkaline affinity, whereas most of younger granites (YG) have a peraluminous character and slightly metaluminous and peralkaline [15, 16]. Ages obtained for Older Granites from the Eastern Desert are younger than 750 Ma [17]. The Younger granites are of wide distribution across the ED, where they form high relief bold mountains. They intrude the earlier exposed rocks with sharp contacts and they commonly possess steep walls and oval or elongated outlines. They enclose mafic xenoliths, enclaves and roof pendants of country rocks with sharp contacts with the enclosing granitic rocks. The younger granites are either of calc-alkaline character, LILE-enriched, highly fractionated I-type granites, or alkaline rocks of A-type character. Commonly, the trace element characteristics for YG are marked by enriched contents of K, Rb, Ta, Th, Nb and Zr and depletion in Sr., Ba, P and Ti. They are enriched in the HFSE, Nb, Ta, Zr, Hf, Y, U, Th and total REEs and relatively depleted in Ba, Sr. with LREE-enriched to almost flat and prominent negative Eu anomaly. The emplacement of the Egyptian late- to post-tectonic younger granites covers a time span between 600 and 550 Ma, [18] or 600 and 475 Ma [19].

The Wadi El Bohlog–Wadi Kam Amiri region in the central eastern desert of the Egypt is displayed in Fig. 1a. In the same figure, performed by using a thematic mapper landsat photos, are also reported the rock samples collected. Figure 1b is the geology map of the examined area, with the principal rock units, from oldest to youngest: serpentinites and talc carbonates, older metavolcanics, metasediments, younger metavolcanics, syn to late orogenic granites, post-orogenic granites, dykes (aplitic and basaltic), and wadi deposits (mixed gravels and sands). The granite pluton (intrusive igneous rock) contains post-orogenic granites (Pan-African Orogeny). This pluton is an oval-shaped body with a diameter of 6 to 8 kms and a peak elevation of 982 m above sea level [4]. It is a prominent circular geographic feature traversed by a major wadi that runs northwest to southeast. This pluton intrudes the serpentinites, metasediments, metavolcanics and syn-tectonic granitoids with typical intrusive contact. Numerous NE-trending basic dikes extrude them. Granites were altered in the research area. There are two types of altered granites: the least silicified granite and the highly silicified granite. The sheared and hydrothermally altered sections of the main pluton of post-orogenic granites, especially near the contact with the metasediments, represent the least desilicified granites [5].

2.2 Sampling, mineral and radioactive measurement

N° 31 samples of post-orogenic granites were collected in the Wadi El Bohlog–Wadi Kam Amiri area of Egypt desert (Fig. 1a). About 250 g of each sample were kept in labelled plastic bags and transferred to laboratory. The samples were powdered, pulverized, subdivided, and segregated to concentrate the heavy minerals using a heavy liquids separation technique applying bromoform (specific gravity 2.85 gm/cm^3) [20]. A hand magnet was used to separate the magnetite. The heavy mineral parts were fed through a Frantz Isodynamic Magnetic Separator (Model L-1) with a side tilt of 5° and a forward slope of 20°, in order to remove the residual magnetite and create numerous magnetic fractions at 0.2, 0.5, 0.7, 1, and 1.5 amperes. Minerals were identified using an environmental scanning electron microscope (ESEM) with EDX (voltage, 25–30 keV; beam diameter, 1–2 mm; counting time, 60–120 s) assistance after being selected under a binocular microscope [21]. To determine the radiological hazard indexes, the natural radioactive content of these samples was investigated. The radioelement of ^{238}U, ^{232}Th, and ^{40}K were detected. To obtain the secular equilibrium of radionuclides in the ^{238}U and ^{232}Th series, the samples were sealed to avoid leakage of ^{222}Rn and ^{220}Rn, and, then, measured after 1 month. A gamma spectrometer with a 76×76 mm^2 NaI(Tl) crystal and a voltage level powered photomultiplier tube (PMT) were used for rapid, non-destructive, and effective radiation detection in the granitic rocks (GR) samples [22]. The pulse management and information analysis apparatus included a multi-channel analyzer and a spectroscopic amplifier, and it was connected to GammaVision software for the analysis of the spectra. Gamma energies from the nuclei of the ^{238}U, ^{232}Th, and ^{40}K are 1764 keV, 2614 keV, and 1460 keV, respectively. Energy and efficiency calibrations were obtained using three multi-γ-ray sources with known activity and energy values from 59.5 to 1332.5 keV. The range of calibration efficiency is varied from 0.5 to 2%. The granitic samples were measured for 2000s using the MDAs of 2, 4, and 12 Bq kg^{-1} for ^{238}U, ^{232}Th, and ^{40}K, respectively. Table 1 shows the commonly used radiological hazard indexes estimated in the present study [23].

3 Results and discussion

3.1 Mineral analysis

The ESEM data and the mineralogical investigation of post-orogenic granites samples revealed the existence of the following mineral groups: i. radioactive minerals (uranothorite and thorite); ii. radio and rare-earth bearing minerals (zircon and xenotime); secondary uranium minerals (kasolite) [24]. The mineral uranothorite [(Th,U)SiO$_4$] is one of the most prevalent thorium silicates. Uranothorite

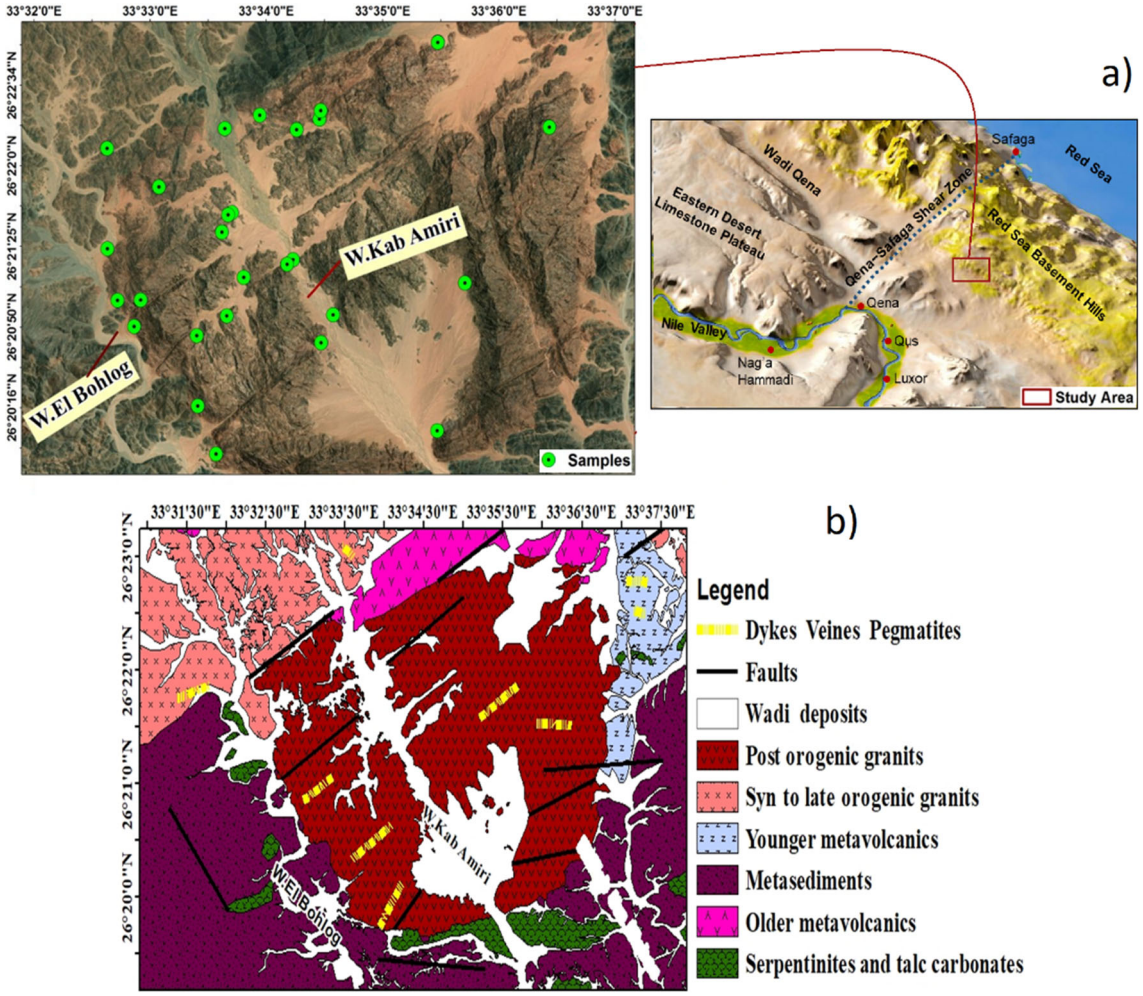

Fig. 1 Wadi El Bohlog–Wadi Kab Amiri area, central eastern desert of Egypt: **a** location map, **b** geologic map

Table 1 Used radiological hazard indexes for granitic rock of Wadi El Bohlog – Wadi Kam Amiri region of Egypt

Parameter	Definition	Formula
Absorbed dose rate D_{air} (nGy/h)	Dose rate exposure in the air at 1 m from radiation sources due to the concentrations (A) of ^{238}U, ^{232}Th and ^{40}K	$D_{air} = 0.462\ A_U + 0.604\ A_{Th} + 0.0417\ A_K$
Outdoor annual effective dose AED_{in} (mSv/y)	Monitor of the radiation exposure indoor and outdoor during a stationary period (1 y)	$AED_{out} = D_{air}$ (nGy/h) $\times 0.2 \times 8760$ (h/y) $\times 0.7$ (Sv/Gy) $\times 10^{-6}$ (mSv/nGy)
Indoor annual effective dose AED_{out} (mSv/y)		$AED_{in} = D_{air}$ (nGy/h) $\times 0.8 \times 8760$ (h/y) $\times 0.7$ (Sv/Gy) * 10^{-6} (mSv/nGy)
Excess Lifetime Cancer Risk—*ELCR*	Probability of developing cancer over a lifetime at a given exposure level	$ELCR = (AED_{in} + AED_{out}) \times 70\ y \times 0.05$

grains, according to ESEM microphotograph and EDX spectrum in Fig. 2a, are mostly made up of Si (11.8 Wt%), U (13.85 Wt%), and Th (74.35 Wt%) [10]. The mineral thorite ($ThSiO_4$) can be found as rounded to sub-rounded grains, prismatic crystals, and black to brownish black grains. Pegmatites, quartz barite veins, granites, hydrothermal deposits, and syenites are just a few of the rock types and geologic conditions where it can be found as an accessory mineral. It is considered a primary mineral. EDX analyses of thorite minerals containing Th (49.79 Wt%) and U (13.59 Wt%), representing the main constituents with the Si (16.48 Wt%) (Fig. 2b) [13]. The mineral zircon ($ZrSiO_4$), in plutonic igneous rocks, is a common accessory mineral. The presence of radioactive atoms may play a significant role in the metamict state (crystal structure breakdown) in zircon. Zircon appears as short and long euhedral

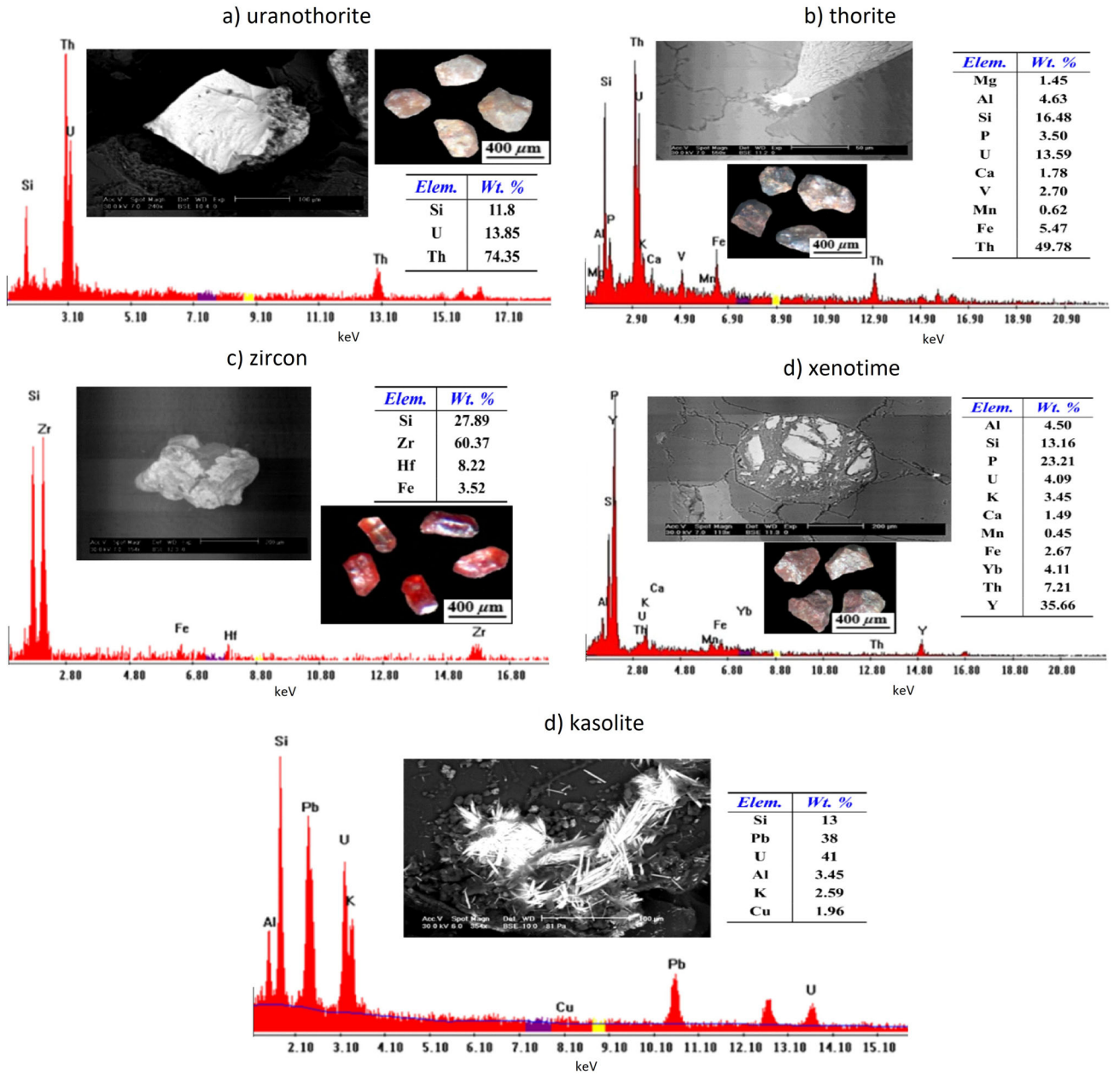

Fig. 2 Binocular microscope images, backscattered electron (BSE) images and EDX analysis for: **a** uranothorite mineral, **b** thorite mineral, **c** zircon mineral, **d** xenotime mineral, **e** kasolite mineral

prismatic crystals under a binocular microscope. These crystals are reddish brown in color and range in transparency from opaque. Zircon grain is mostly constituted of Zr (60.37 Wt%), Si (27.89 Wt%), Hf (8.22 Wt%), and Fe (3.52 Wt%), according to ESEM microphotographs and EDX studies (Fig. 2c) [24]. The mineral xenotime (YPO_4) is a rare earth element orthophosphate mineral that includes as an accessory mineral in granitic rocks, rhyolites, pegmatites, and metapelites. It is the most abundant phosphorous carrying mineral that contains substantial levels of heavy rare-earth elements. In the investigated rock, xenotime is found in bigger forms such as anhedral aggregates and granular grains that range in color from dark brown to reddish brown [11]. Figure 2d depicts the results of an investigation of a xenotime mineral using a binocular microscope, a scanning electron microscope (SEM/EDX), and back-scattered electron imaging (BSE). EDX analysis of some xenotime mineral grains shows that they are composed mainly of Al (4.50 Wt%), Si (13.16 Wt%), P (23.21 Wt%), U (4.09 Wt%), K (3.45 Wt%), Ca (1.49 Wt%), Mn (0.45 Wt%), Fe (2.67 Wt%), Yb (4.11 Wt%), Th (7.21 Wt%) and Y (35.66 Wt%). The mineral kasolite ($Pb(UO_2)(SiO_4)H_2O$) is a significant hydrated uranyl silicate mineral phase. It is a secondary mineral that results from the reaction of secondary uranium minerals with meteoric water that contains silica. The monoclinic structure and resinous or oily sheen of kasolite set it apart [13, 24]. This mineral has a Mohs hardness of 4–5, making it comparatively tougher than other secondary uranium minerals. With the occasional appearance of

Table 2 Statistics of radiometric results on 31 samples of granitic rock in Wadi El Bohlog – Wadi Kab Amiri area

	Minimum	Maximum	Average	Standard deviation	Coefficient of variability (%)
eU (ppm)	1	15	5.7	6.1	92
eTh (ppm)	1.3	50	14.4	11.8	82
^{40}K (%)	0.2	5	3.2	1.6	51
^{238}U (Bq/kg)	12.35	185.25	70.40	75.33	92
^{232}Th (Bq/kg)	5.27	203	58.46	47.90	82
^{40}K (Bq/kg)	62	1565	1002	501	51

iron oxide staining, kaolite is typically found as lath- to needle-shaped collected crystals (SEM/EDX) and back-scattered electron imaging (BSE) (Fig. 2e). The results of kasolite's EDX examination reveal the presence of of Si (13 Wt%), Pb (38 Wt%) U (41 Wt%), Al (3.45 Wt%), K (2.59 Wt%) and Cu (1.96 Wt%).

3.2 Radioactivity content

Table 2 summaries the results of the content of natural radionuclides in post-orogenic granites samples. Hereby, the terms eU or eTh denote equivalent of ^{238}U or of ^{232}Th, meaning the natural radiation emitted by all radionuclides belonging to the decay series of ^{238}U (eU = ^{226}Ra = ^{214}Bi) and ^{232}Th (eTh = ^{228}Th = ^{208}Tl), which occur in the analyzed samples [25]. This fact is performed assuming the secular equilibrium of radionuclides, obtained by sealing the samples to avoid leakage of ^{222}Rn and ^{220}Rn, and, then, measuring the samples after 1 month. In particular, eU ranged from 1 to 15 ppm, eTh ranged from 1.3 to 50 ppm, ^{40}K ranged from 0.2 to 5% with averages of 5.7 ppm, 14.4 ppm and 3.2%, respectively. The following conversions can be used to obtain the radionuclide content into activity concentration [6, 26]: 1% of ^{40}K in rock corresponds to 313 Bq/kg; 1 ppm eU in rock is 12.35 Bq/kg of ^{238}U; 1 ppm of eTh in rock is 4.06 Bq/kg of ^{232}Th.

The obtained results in Table 2 show high values in accordance with the literature of post-orogenic granites: 3–6 ppm for eU and 8–23 ppm for eTh [2, 4, 5, 27]. According to the work [28], in Table 2 in also reported the coefficient of variability (CV) that determines how statistically significant are the data from gamma-ray spectrometry. According to the equation from [20], i.e., CV $\% = (\sigma/X) \times 100$ with σ the standard deviation and X the arithmetic mean, the data tend to have a normal distribution in the study region if the CV is less than 100%. In Table 2, CV determines the degree of distributions homogeneity of the several radioelement for the post-orogenic granite units. Table 2 shows that ^{40}K distributions are moderately homogeneous compared to eU and eTh that indicate lower levels of homogeneity. These values can be explained by the presence of different minerals during geological formations in post-orogenic granite samples [29] (Sect. 3.1). Figure 3a illustrates the relationships between eTh-eU, showing a very strong relationship ($R^2 = 0.77$). This aspect suggests that uranium and thorium mineralization are controlled by magmatic processes. Figure 3b and c show the weak relation of ^{40}K with eU and eTh, respectively: this may be attributed to the alteration processes of feldspars.

The relationship between the radioelements exhibits that their distribution are not only magmatic but also hydrothermal. Moreover, in Fig. 4d the eTh/^{40}K versus eTh/eU shows that the majority of the samples under evaluation are located in the fixed-U sector, indicating that using them as building material or decorations could be risky [30]. In the examined post-orogenic granites, the radionuclide activity concentrations of ^{238}U, ^{232}Th and ^{40}K in Bq/kg are also displayed in Table 2. The range of ^{238}U, ^{232}Th and ^{40}K activity concentrations are 12.35–185.25 Bq/kg, 5.27–203 Bq/kg and 62–1565 Bq/kg, respectively. The average values with standard deviation of ^{238}U, ^{232}Th and ^{40}K activity concentrations are 70.40 ± 75.33 Bq/kg, 58.46 ± 47.90 Bq/kg and 1002 ± 501 Bq/kg, respectively. The obtained results show that the average data for ^{238}U, ^{232}Th and ^{40}K are greater than the worldwide average data, which are 33, 45, and 412 Bq/kg, respectively [31].

The studied materials have such high radioactive levels as a result of weathering, leaching, modification, and aeration processes. A buildup of radioactive minerals, such as uranothorite, zircon, monazite, allanite, clay, and feldspar, among others, is the cause of the high concentration of ^{238}U, ^{232}Th and ^{40}K in the post-orogenic granite samples [11, 27, 30]. The skewness and kurtosis parameters were computed for the radioelements in the 31 samples, in order to determine the asymmetry distribution and the heaviness of a distribution's tails relative to a normal distribution. The skewness values of ^{238}U (2.31) and ^{232}Th (1.31), as well as the kurtosis values of ^{238}U (7.76) and ^{232}Th (1.91) are positive. Whereas for ^{40}K the skewness is -0.97 and kurtosis is -0.61. The frequency distribution of ^{238}U, ^{232}Th and ^{40}K in the 31 samples are in Fig. 4.

3.3 Radiological hazard indexes

The radiological hazard indexes determine the assessment of post-orogenic granites from Wadi El Bohlog–Wadi Kab Amiri of Egypt used as construction materials: in Table 3 are reported the results. The absorbed dose rate D_{air} varied among 13 and 251 nGy/h, with a mean value of 114 nGy/h that is greater than the UNSCEAR recommended amount of 58 nGy/h [31]. Consequently, the produced photons from post-orogenic granites will damage humans, and long-term exposure to radioactive material will have negative health

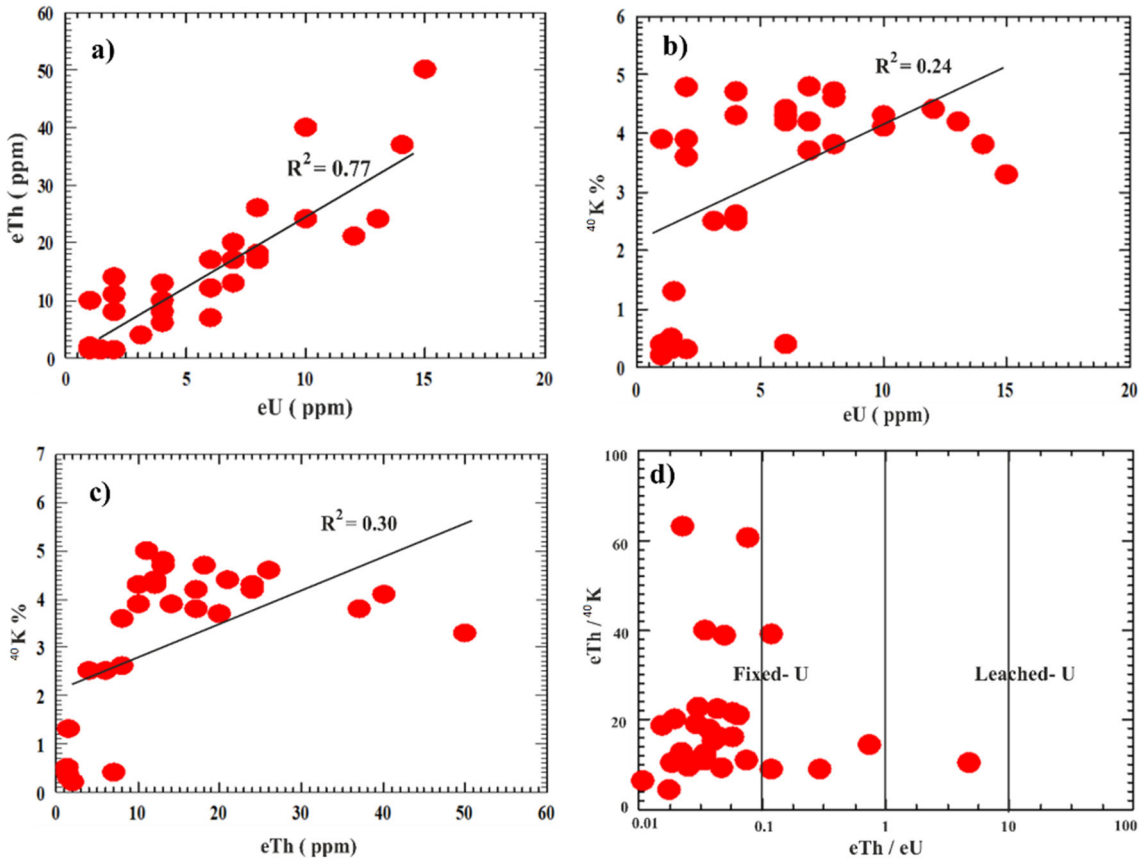

Fig. 3 Radiometric analysis in 31 samples of granitic rocks in Wadi El Bohlog–Wadi Kab Amiri region: correlations between **a** eTh and eU, **b** ^{40}K and eU, **c** ^{40}K and eTh, **d** eTh/^{40}K and eTh/eU

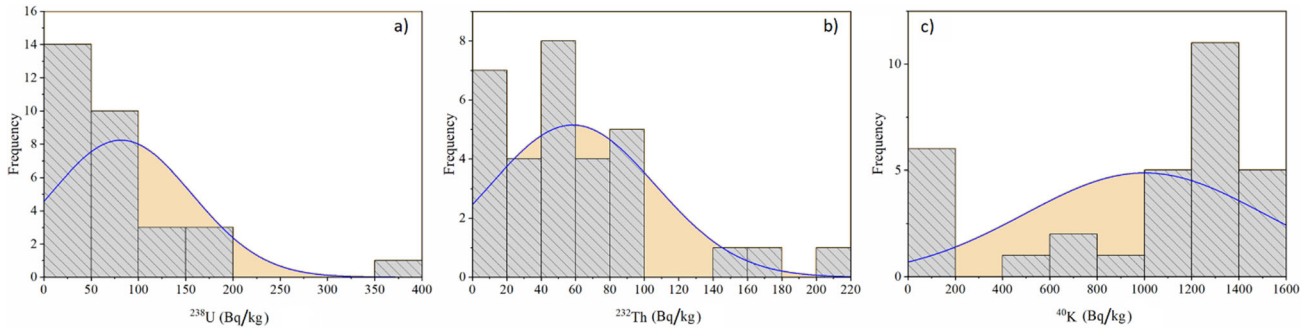

Fig. 4 Radiometric analysis in 31 samples of granitic rocks in Wadi El Bohlog–Wadi Kab Amiri region: frequency distribution of the activity concentration (Bq/kg) of **a** ^{238}U, **b** ^{232}Th, **c** ^{40}K

consequences. Indoor and outdoor annual effective dose AED_{in} and AED_{out} mean values are 0.56 and 0.14 mSv/y, respectively, which are greater than the allowable averages of 0.40 mSv/y (indoor) and 0.06 mSv/y (outdoor) [31]. This means that long-term low-level exposure has negative health repercussions such as tissue degeneration, DNA in genes, cancer, or cardiovascular disease [32]. The excess lifetime cancer risk (ELCR), i.e., the probability of developing cancer over a lifetime at a given exposure level, is found over the worldwide average limit of ranges from 0.28 to 5.38 with a mean value of 2.45· The mean value is significantly greater than the reference limit of 1.45 [23].

3.4 Pearson correlation, principal component and hierarchical cluster analysis

Correlations between ^{238}U, ^{232}Th and ^{40}K activity concentrations and radiological hazard indicators in the 31 post-orogenic granites of Wadi El Bohlog–Wadi Kab Amiri area in Egypt are studied by using the Pearson correlation analysis (PC) (Table 4). The PC analysis classified the correlations into four categories: weak (0.3–0.49), moderate (0.5–0.69), high (0.7–0.9), and extremely strong

Table 3 Radiological hazard indexes in the 31 granitic rocks samples of Wadi El Bohlog – Wadi Kab Amiri area

	D_{air} (nGy/h)	AED_{out} (mSv/y)	AED_{in} (mSv/y)	ELCR
Average	114	0.14	0.56	2.45
Standard deviation	67	0.08	0.33	1.43
Minimum	13	0.02	0.06	0.28
Maximum	251	0.31	1.23	5.38

Table 4 Pearson correlation among radionuclides content and radiological hazard indexes in the 31 samples of granitic rock from Wadi El Bohlog – Wadi Kab Amiri region of Egypt

	^{238}U	^{232}Th	^{40}K	D_{air}	AED_{out}	AED_{in}	ELCR
^{238}U	1	0.46	0.26	0.80	0.80	0.80	0.80
^{232}Th	\\	1	0.55	0.85	0.85	0.85	0.85
^{40}K	\\	\\	1	0.69	0.69	0.69	0.69

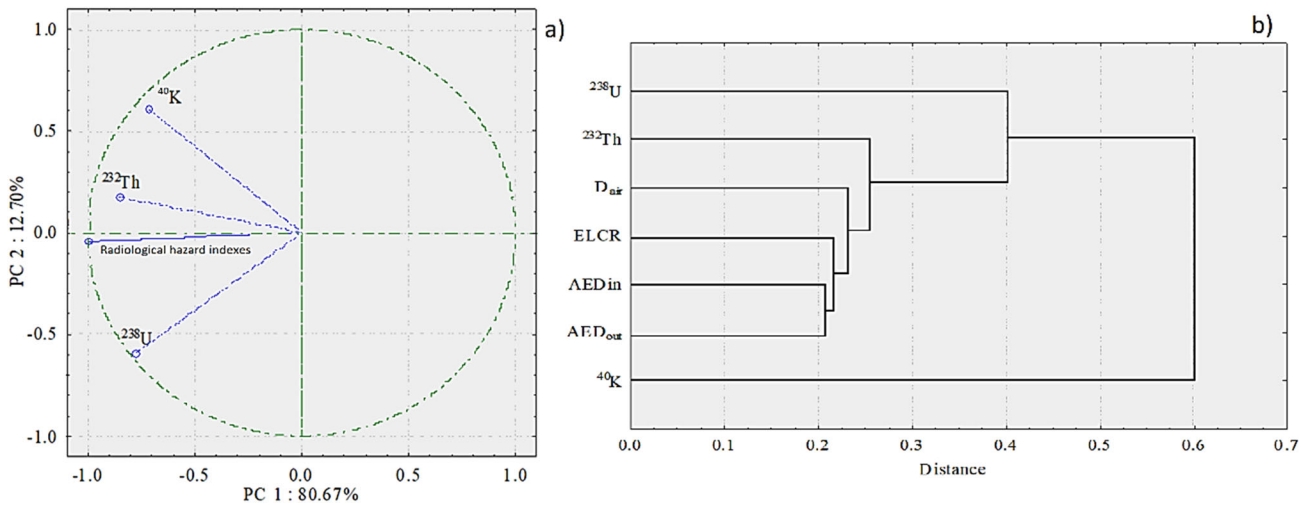

Fig. 5 Graphical representation of PCA analysis (**a**) and dendrogram from hierarchical cluster analysis (**b**) of radionuclides content and radiological hazard indexes in 31 granitic rocks from Wadi El Bohlog–Wadi Kab Amiri

(>0.9) [27]. Weak correlations are between ^{238}U with ^{40}K ($R^2 = 0.26$) and ^{232}Th ($+R^2 = 0.46$). The correlation between ^{40}K and ^{232}Th is moderate (0.55). These low correlations are explained by the investigation into the uranium and thorium mineral enrichment of post-orogenic granites (Sects. 3.1 and 3.2) [5, 11]. Table 4 shows that there are high connections between ^{238}U and ^{232}Th with the radiological hazard indexes ($\geq 80\%$). As a result, the main causes of the negative health effects associated with the gamma radiation produced from the post-orogenic granites are uranium and thorium.

The principal component analysis (PCA) is also performed to further analyze the relation among the ^{238}U, ^{232}Th and ^{40}K activity concentrations and radiological hazard indicators in the 31 post-orogenic granites of Wadi El Bohlog–Wadi Kab Amiri area in Egypt [33]. Component 1 (PC1) and component 2 (PC2) are obtained and shown in Fig. 5a. From the figure is clear that PC1 is heavily loaded with the activity concentrations of ^{238}U and ^{232}Th in relation to all radioactive components (80.67%). In fact, in the post-orogenic granites at the work location, ^{238}U and ^{232}Th were the primary naturally occurring radioactive contributions. Contrarily, the PC2 load for ^{40}K (12.70%). This is also evident in the radiological hazard indexes behavior [27, 34]. The hierarchical cluster analysis (HCA) is a data categorization system that use multivariate algorithms to distinguish between several types of data. The Euclidean distance between radiological hazard indexes and radioactive activity concentrations is performed [35]. The HCA output is the dendrogram of the investigated data in Fig. 5b, obtaining three major clusters. ^{238}U is present in cluster I, ^{232}Th is present in cluster II, along with radiological hazard indexes, and ^{40}K is present in cluster III. According to HCA, radioactive concentrations, particularly uranium and thorium, are associated with the radioactivity of post-orogenic granites [29].

3.5 Distribution maps of the radioelements

The results of eU (ppm), eTh (ppm) and ^{40}K (%) were utilized to create color contour maps, i.e., maps on which the shape of the land surface is shown by contour lines that join points of equal elevation [36]. The eU contour map (Fig. 6a) shows that values ranged from 1.4 to 16.3 ppm over the post-orogenic granites in the study area. The high values of eU over the post-orogenic granites range between 6.6 and 16.3 ppm, which located at central and southern parts of the study area due to the presence of radioactive

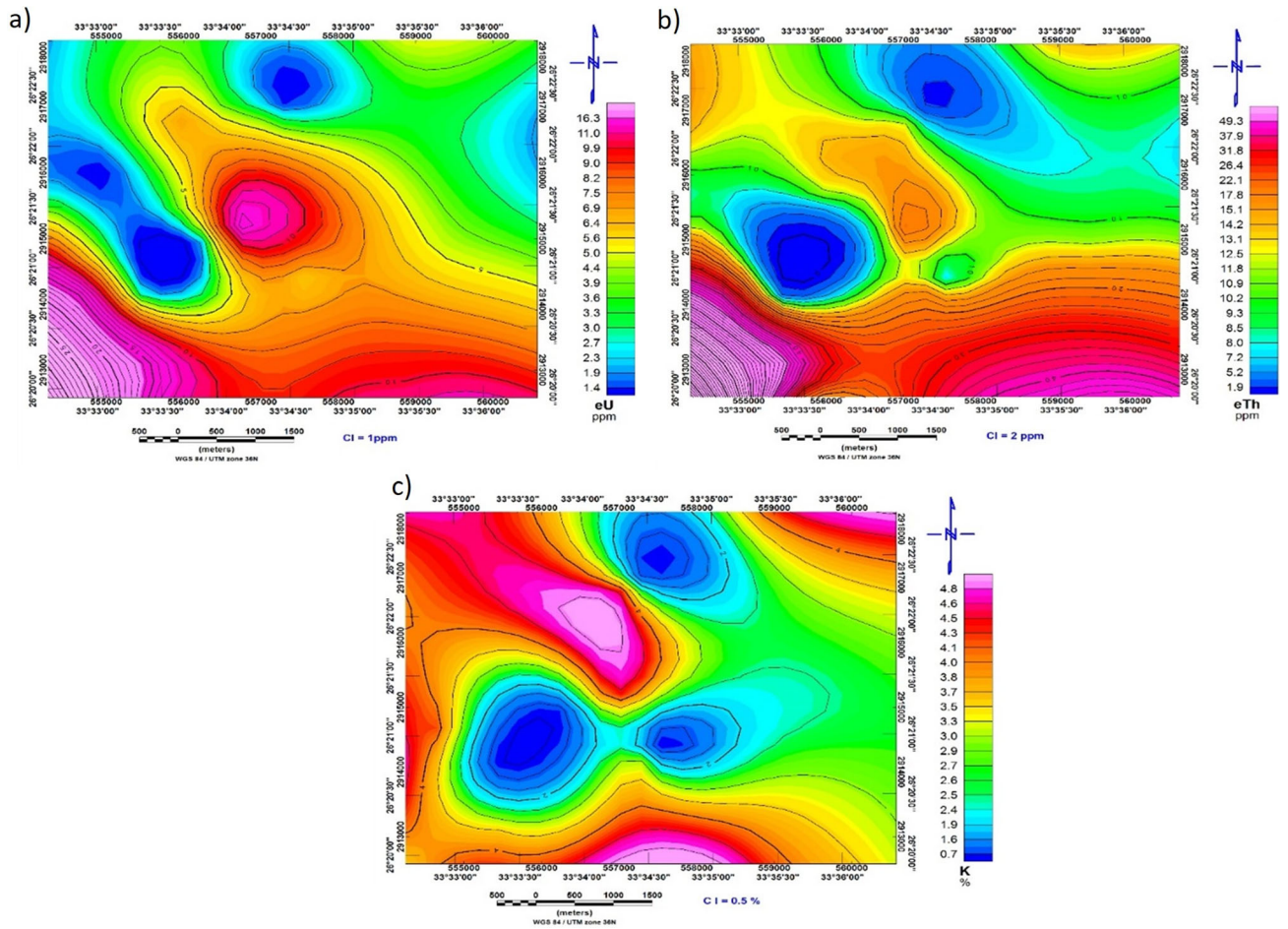

Fig. 6 Color contour map of eU in ppm (**a**), eTh in ppm (**b**), ^{40}K in % (**c**) in the 31 granitic samples from Wadi El Bohlog – Wadi Kab Amiri region of Egypt

accessory mineral (e.g., uranothorite, zircon, xenotime and kasolite) [5, 37]. The low values of eU are located at the northeastern and northwestern parts. In general, the pattern of eU anomalies has a marked tendency in the NNW-SSE and NW–SE direction. The eTh contour map (Fig. 6b) shows that the post-orogenic granites have the highest values in the southern and northwestern parts of study area, that range between 13.1 ppm and 49.3 ppm, suggesting that the distribution of both uranium and thorium are governed by magmatic processes and presence of uranothorite and thorite minerals [13]. The lowest levels of eTh in post-orogenic granites range between 13.1 and 1.9 ppm, which located at the northeastern and the central of western parts. The major trend of anomaly is NNW-SSE and E-W direction. The ^{40}K contour map(Fig. 6c) reflects two levels of concentrations. The lowest one ranges between 0.7% and 3.5%, and it is represented in the centeral, northern, eastern and western parts of the area. The second level is a high zone having values ranged 3.5% to 4.8%. This zone is primarily concentrated in the northeastern, northwestern and southern parts of the study area due to K-metasomatism alteration processes of plagioclase [27, 37].

The distribution map of ^{238}U, ^{232}Th and ^{40}K is performed by a color composite map (Fig. 7), i.e., a ternary radioelement map controlling red, green, and blue in accordance with the activity concentration of ^{40}K, ^{238}U and ^{232}Th, respectively, [38]. The colors at each place in the map correspond to different radioelement according to the color variations on the three radioelements. The light zones represent the greater activity concentrations of the three radioelements. The higher light zones are clearly occupied the southern and central parts of the Wadi El Bohlog–Wadi Kab Amiri region of Egypt. The lowest activity concentrations of the three radioelements are located in the black area: central of northern and western parts of the study area. Uranium concentrations are highest in the centre of the study region. The obtained map in Fig. 7 highlights some lithological features of various rock units, in agreement with the geologic map (Fig. 1b) of the Wadi El Bohlog–Wadi Kab Amiri region of Egypt desert [4]. The map aids to identify potential U-Th resources in the study region.

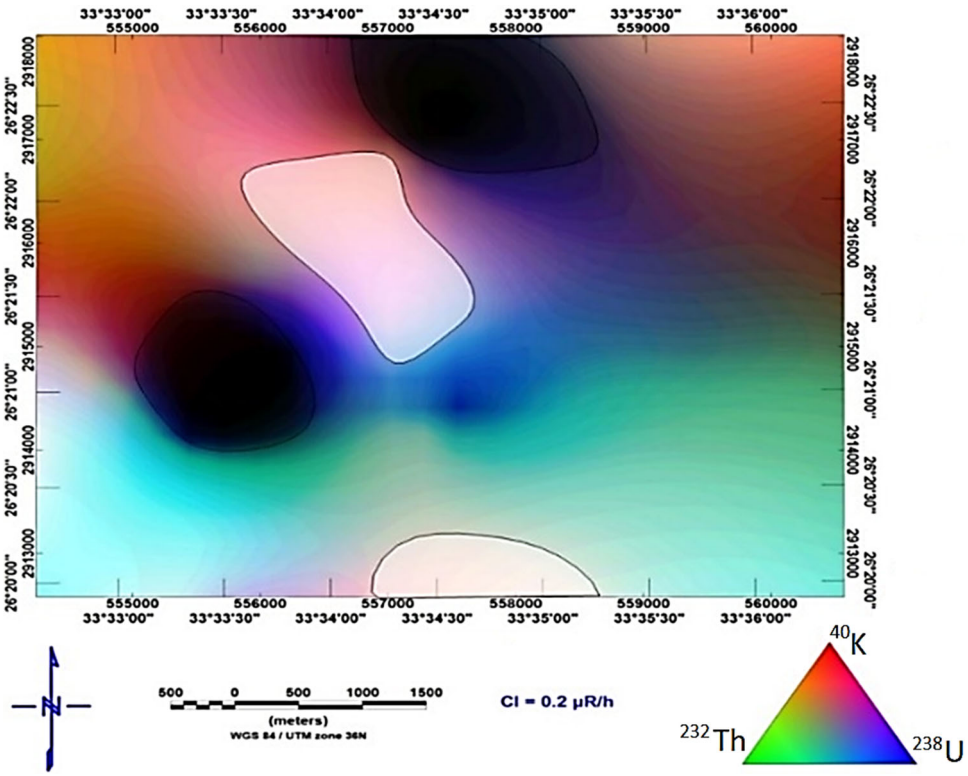

Fig. 7 Color composite map of ^{238}U, ^{232}Th, ^{40}K in the 31 granitic samples from Wadi El Bohlog – Wadi Kab Amiri

4 Conclusion

The spectrometric measurements on 31 post-orogenic granites samples from the Wadi El Bohlog–Wadi Kab Amiri region of desert of Egypt were performed by NaI(Tl) detector. The average of activity concentrations of the natural radionuclides ^{40}K, ^{238}U and ^{232}Th highlight high values over the worldwide limits: ^{238}U with 70.40 Bq/kg, ^{232}Th with 58.46 Bq/kg, ^{40}K with 1002 Bq/kg exceeded the worldwide average limits of 33, 45, 412 Bq/kg, respectively. The radioelements distribution maps reflect: higher zones in the southern and central parts of the region, lower zones sited at the central of northern and western parts of the examined area. The mineralogical investigations by environmental scan electron microscope (ESEM) indicate that the main mineral association of the studied granites include thorite, uranothorite, kasolite, zircon and xenotime. Radiological hazard indexes, i.e., absorbed dose rate, annual effective dose and excess lifetime cancer risk are computed and found to be higher than the worldwide limits. The presence of bearing radioactive minerals in the post-orogenic granites donates the high values of natural radionuclides, and, hence, high radiological hazard indexes values, according to the statistical investigation. As a result, the post-orogenic granites are unsuitable for utilizing in building fields.

Acknowledgements The authors extend their appreciation to the Deanship of the Scientific Research at King Khalid University for funding this research through the Research Group Program under the Grant No. RGP2/515/44.

Data Availability Statement This manuscript has associated data in a data repository. [Authors' comment:The datasets generated during and/or analysed during the current study are available from the corresponding author on reasonable request.]

Declarations

Conflict of interest Nothing to declare.

References

1. M.A. Akpanowo, I. Umaru, S. Iyakwari, E.O. Joshua, S. Yusuf, G.B. Ekong, Sci. African **10**, e00561 (2020)
2. S. Sivakumar, A. Chandrasekaran, R. Ravisankar, S.M. Ravikumar, J.P.P. Jebakumar, P. Vijayagopal, I. Vijayalakshmi, M.T. Jose, J. Taibah Univ. Sci. **8**, 375–384 (2014)
3. G. La Verde, F. Ambrosino, M. Ragosta, M. Pugliese, Appl. Sci. **13**(8), 4701 (2023)
4. M.A. Wetait, A.F. El Hadary, A.A. Khamies, B.A. Zoheir, S.M. Elalfi, Al Azhar Bull. Sci. **25**(1), 63–73 (2014)
5. A.M. El Mezayen, E.M. Ibrahim, M.G. El-Feky, S.M. Omar, A.M. El-Shabasy, S.A. Taalab, Int. J. Environ. Anal. Chem. **102**, 970–986 (2020)

6. S.A. Taalab, W.H. Mohamed, S.A. Shetaia, M. Al Meshari, Y. Alzamil, A. Abanomy, A.R. Alyahyawi, A. El-Taher, J. Environ. Sci. Health Part A **58**, 326–341 (2023)
7. M. Ivanovich, R.S. Harmon, Clarendon Press, Oxford pp. 910 (1992)
8. D. Scholz, D. Hoffmann, E&G Quat.1 Sci. J. **57**, 52–76 (2008)
9. U. Aswathanarayana, *Principles of nuclear geology* (Oxonian Press. Pvt. Ltd., New Delhi, India, 1985)
10. L. Xinwei, W. Lingqing, J. Xiaodan, J. Radioanal. Nucl. Chem. **267**, 673–699 (2006)
11. R.M. Abd El Rrahman, S.A. Taalab, Z.Z. Alfull, M.S. Mohamed, M.I. Sayyed, N. Almousa, M.Y. Hanfi, Minerals **12**, 353 (2022)
12. F. Ambrosino, G. La Verde, C. Sabbarese, V. Roca, A. D'Onofrio, M. Pugliese, Isot. Environ. Health Stud. **59**(2), 192–201 (2023)
13. M.M. El Dabe, A.M. Ismail, M. Metwaly, S.A. Taalab, M.Y. Hanfi, A. Ene, Materials **15**, 1224 (2022)
14. R.J. Stern, Ann. Geol. Surv. Egypt **9**, 9–13 (1979)
15. G.A. El Bahariya, Geochemistry (IntechOpen) **10**, 95904 (2021)
16. F. Finger, W. Dorr, A. Gerdes, M. Gharib, M. Dawoud, Mineral. Petrol. **93**, 153–183 (2008)
17. A. Andresen, M.M.A. El-Rus, P.I. Myhre, G.Y. Boghdady, F. Corfu, Int. J. Earth Sci. **98**, 481–497 (2009)
18. R.J. Stern, C.E. Hedge, Am. J. Sci. **285**, 7–127 (1985)
19. K.A. Ali, A. Andresen, R.J. Stern, W.I. Manton, S.A. Omar, A.E. Maurice, Geol. Mag. **149**, 783–797 (2012)
20. K. Fujiwara, S. Yamasaki, H. Nagatsuka, J. Geol. Soc. Japan **127**(12), 727–732 (2021)
21. F. Schröter, E. Schmidt, Powder Technol. **330**, 80–92 (2018)
22. J. Guillén, J.J. Tejado, A. Baeza, J.A. Corbacho, J.B. Muñoz, J. Environ. Radioact. **132**, 81–88 (2014)
23. I.K. Ahmed, H.N.B. Khalaf, F. Ambrosino, M.Y.A. Mostafa, J. Radioanal. Nucl. Chem. **329**(3), 1237–1245 (2021)
24. A.S. Aykamiş, S. Turhan, F.A. Ugur, U.N. Baykan, A.M. Kiliç, Radiat. Prot. Dosim. **157**, 105–111 (2013)
25. G. Roveratti, D.M. Bonotto, Appl. Radiat. Isot. **188**, 110399 (2022)
26. M.Y. Hanfi, M.S. Masoud, F. Ambrosino, M.Y.A. Mostafa, Appl. Radiat. Isot. **173**, 109705 (2021)
27. A. Abbasi, Radiat. Prot. Dosim. **155**, 335–342 (2013)
28. D.D. Sarma, G.S. Kock, Math. Geol. **12**(2), 99–114 (1980)
29. M.R. Khattab, Phys. Chem. Earth Parts A/B/C **128**, 103204 (2022)
30. A.M.A. Sadek, A.H.A. Abbas, A.M. El-Sherif, Nucl. Sci. **4**, 37–45 (2015)
31. UNSCEAR Report, United Nations Publication. Sales No. E.10.XI.3 (2008)
32. M. Durante, G. Gialanella, G. Grossi, M. Pugliese, P. Scampoli, T. Kawata, N. Yasuda, Y. Furusawa, J. Radiat. Res. **43**, S107–S111 (2002)
33. C. Sabbarese, M.L. Feola, F. Ambrosino, V. Roca, A. D'Onofrio, G. La Verde, V. D'Avino, M. Pugliese, V. Festa, Environments **9**(7), 82 (2022)
34. R. Ravisankar, J. Chandramohan, A. Chandrasekaran, J.P. Prakash, I. Vijayalakshmi, P. Vijayagopal, B. Venkatraman, Mar. Pollut. Bull. **97**(1–2), 419–430 (2015)
35. M.J. Abedin, M.R. Karim, M.U. Khandaker, M. Kamal, S. Hossain, M.H.A. Miah, D.A. Bradley, M.R.I. Faruque, M.I. Sayyed, Radiat. Phys. Chem. **177**, 109165 (2020)
36. A. Al-Lawati, A.S.S. Dorvlo, J.A. Jervase, Energy Convers. Manag. **44**(5), 691–705 (2003)
37. M.G. El-Feky, Chin. J. Geochem. **30**, 430–443 (2011)
38. J.S. Duval, Geophysics **48**(16), 722–735 (1983)